Impact of Moisture on the Properties of $LiNi_xCo_yMn_{1-x-y}O_2$ (NMC) Cathodes for Lithium-Ion Batteries

Undergraduate Honors Thesis

Presented in Partial Fulfillment of the Requirements for Graduation with Distinction in the Department of Mechanical Engineering at The Ohio State University

Liang Dong

April 2018

Advisor: Jung-Hyun Kim, Ph.D.

Abstract

Lithium-ion battery (LIB) are in high demand for portable electronic devices and EV today. Much attention has been paid to cathode material since it governs the energy density of LIB. $LiNi_xCo_yMn_{1-x-y}O_2$ (NMC) materials with various molar ratios of Ni: Mn: Co is now popular options for cathode materials for its lower cost, less toxicity and higher specific capacity comparing to traditional cathode materials such as $LiCoO_2$. However, the material suffers from performance degradations in contact with moisture in the air. Although this is a particularly important problem, we still have a lack of fundamental understanding about its failure mechanism. Based on literature review, we hypothesized that a high oxidation-state Ni^{3+} in NMC will readily react with moisture to lower its oxidation state into Ni^{2+} and lower the electrochemical capacity of NMC. To prove the hypothesis, we selected and investigated various NMC with different Ni contents: $(1).\ LiNi_{1/3}Co_{1/3}Mn_{1/3}O_2$, $(2).\ LiNi_{0.5}Co_{0.3}Mn_{0.2}O_2$, $(3).\ LiNi_{0.6}Co_{0.2}Mn_{0.2}O_2$, (4) $LiNi_{0.8}Co_{0.1}Mn_{0.1}O_2$. We stored each type of NMC powder under three different conditions: (i) dry glovebox, (ii) 2% moisturized chamber, and (iii) water. Then, we characterized the samples by using X-ray Powder Diffraction (XRD), Fourier Transform Infrared Spectroscopy (FTIR), and electrochemical performance test from coin type battery cells. Testing results from the same type of powder in different conditions will be compared with each other to find how the extent of moisture affects the powders, while testing results from different powders in the same condition will be compared with each other to find how the amount of Ni content affects moisture impact.

Acknowledgments

Many people had a hand in the success of this research project. First, I must thank my advisor, Dr. Jung-Hyun Kim. My accomplishments over this past year are results of his continuous support, valuable advice, and absolute trust. He kept my project organized and communication between us efficient by having weekly reports and meetings. Also, he always responds to emails quickly even on weekends, which brings great convenience to me. There aren't enough pages for me to express how thankful I am for Dr. Kim's unselfish dedication.

I owe a huge thank you to the graduate students in the Energy Innovation Lab, especially Cody O'Meara and Chan-Yeop Yu. Cody was almost my second advisor. He was kind and patient enough to guide me through specific experiments and was understanding enough to answer most of the questions I have towards the research topic. Chan-Yeop Yu also helped me a lot during the past year. For example, he helped me get familiar with the lab facilities, set up some experiments and do the XRD refinement. They both sacrificed countless hours of their very limited free time to help me accomplish this project.

A big thank you also goes to my fellow undergraduate researchers in the Energy Innovation Lab, who provided me valuable suggestions, constructive criticisms, and encouragements. With their company, I avoided many mistakes during experiments and documentation preparation stages. Finally, I want to thank my friends and family, who gave me the courage to break challenges and pursue higher goals. Their expectation is my biggest motivation for going forward.

Table of Contents

List of Figures

List of Tables

Chapter 1: Introduction

Lithium-ion battery (LIB), as its name would suggest, is a type of rechargeable battery in which lithium ions move from the negative electrode to the positive electrode during discharge and back when charging (illustrated in Figure 1). It is a leading contender for portable electronics because of its high energy density, low memory effect, and low self-discharge. The main components of LIB are electrodes, including cathode and anode, electrolyte and separator. The cathode is particularly important since it governs the energy density of the battery.

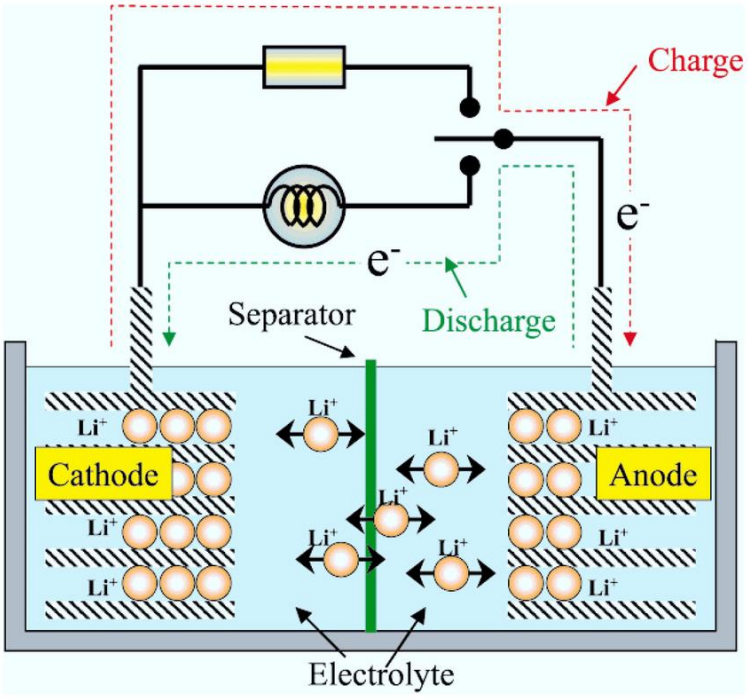

Figure 1: Lithium-ion battery schematic (Nishi, 2001)

Transition metal oxides that can host (i.e., intercalate) Lithium-ion is being used as electrode materials in Li-ion batteries. So far, $LiCoO_2$ has been adopted as the most common cathode material in Li-ion batteries for electronic devices, including camera, cellular phone, and laptop, because it offers many advantages such as the ease of fabrication, good thermal stability, and high energy density. However, there are concerns about $LiCoO_2$, including high cost, high

toxicity, and high safety risks (e.g., fire, explosion, etc). Therefore, $LiNi_xCo_yMn_{1-x-y}O_2$ (NMC) has been selected as an alternative to $LiCoO_2$ after significant research and development (R&D) efforts. This cathode material offers slightly lower energy density and maintains the same crystal structure as $LiCoO_2$, but has great benefits such as lower cost, lower toxicity, less likelihood of safety risks, more cycle life and higher capacity due to the partial Ni and Mn substitutions for Co.

Nowadays, LIBs using NMC as cathodes have been used in the automotive industry. For example, $LiNi_{1/3}Co_{1/3}Mn_{1/3}O_2$ and $LiNi_{0.6}Co_{0.2}Mn_{0.2}O_2$ have been adopted as cathodes for plug-in hybrid electric vehicles (PHEVs). However, NMC materials still have a major problem to be solved, which affects their performance: their contact with moisture in the air can cause performance degradation. Some researchers have started to investigate the moisture impact on NMC materials. According to Cho et al., the surrounding of cathode particle can be contaminated with moisture and CO_2 in the air, which can form LiOH and Li_2CO_3 on the surface (shown in

Figure 2: Surface contamination of Ni-rich materials after exposure in air (Cho, 2014)

Figure 2). Yang et al. also reported the following surface reaction mechanism (Yang, 2004):

$$2Li^+ + CO_3^{2-}/2OH^- \rightarrow Li_2CO_3/2LiOH$$

These residual lithium compounds will consume extra Lithium and impede the diffusion of Li^+ ions during charging and discharging due to their insulating properties, thus deteriorate the electrochemical performance of LIB. (Cho, 2014) Some structural changes of NMCs have also

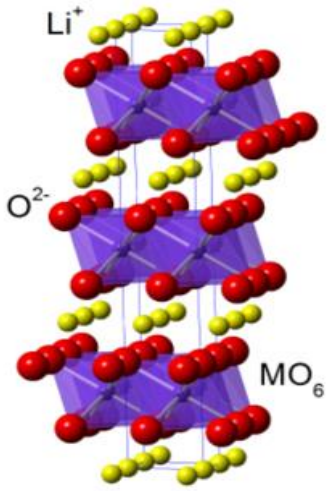

Figure 3: The crystal structure of $LiNi_xCo_yMn_{1-x-y}O_2$ (NMC) cathode (Wang, 2012)

been found after moisture contact. Figure 3 shows the typical crystal structure of NMC cathode, where the blue line indicates the unit cell and the Ni, Mn and Co atoms are randomly distributed on M sites. It was reported by J.-H Park et al. that the Li^+ consumed by surface reactions will leave the Li site vacant, and then accommodate Ni^{2+}, which is reduced from Ni^{3+} in NMC because of the low stability of Ni^{3+} in the FCC octahedral site, due to the similar ionic radius of Li^+ (0.76 Å) and Ni^{2+} (0.69 Å). (Park, 2016) This kind of behavior is called cation mixing.

Based on literature review, we hypothesized that the higher amount of Ni in NMC will cause more occupations of Li site by Ni^{2+}, increase the impedance to the Li^+ movement within the layered structure thus degrades the performance of NMC more severely. To prove this, we need to investigate the degradation mechanisms of different NMCs with different Ni contents.

There are a few papers published that correspond to the moisture impact on NMC, but each has important limitations which have motivated this research project. Particularly, none of them have directly compared deterioration behaviors between NMCs with different Ni contents to prove the significant role of Ni in the NMC failure mechanism after moisture impact.

1.1 Focus of Thesis

The purposes of this research project were to further validate the effect of moisture on NMC and to understand the failure mechanism of NMC materials after moisture impact with the factor of Ni content taken into consideration. We selected and investigated various NMC with different Ni contents: (1) Li $Ni_{1/3}Co_{1/3}Mn_{1/3}O_2$, (2) Li $Ni_{0.5}Co_{0.3}Mn_{0.2}O_2$, (3) $LiNi_{0.6}Co_{0.2}Mn_{0.2}O_2$, (4) $LiNi_{0.8}Co_{0.1}Mn_{0.1}O_2$. To validate the effect of moisture, we stored each type of NMC powder under three different conditions: (i) dry glovebox, (ii) 2.5% moisturized chamber, and (iii) water. Then, we characterized the samples by using X-ray Powder Diffraction (XRD), Fourier Transform Infrared Spectroscopy (FTIR), and electrochemical performance test from coin type battery cells. From the tests, we can get the surface phase information, surface chemical ingredients, charging/discharging performance and impedance information. All those test results can give us an idea of NMC's failure mechanism after moisture impact. Besides that, testing results from the same type of powder in different conditions will be compared with each other to find how the extent of moisture affects the powders, while testing results from different powders in the same condition will be compared with each other to find how the amount of Ni content affects moisture impact.

1.2 Significance of Research

Green and sustainable energy, as well as efficient and economical methods to convert and store energy, has become important work considering the rising environmental issues and dependence on portable and uninterrupted power sources. (Liu, 2016) Many forms of sustainable energy are converted to electrical energy for application and storage, which makes the storage efficiency of electrical energy very critical. Rechargeable batteries such as Lithium-ion battery are

common carriers of electrical energy for portable devices. They store energy as chemical potential in the electrodes, and their energy density is highly dependent on the specific capacity of electrodes. Today, the most advanced type of rechargeable battery that is commercially available is Lithium-ion battery. Its electrodes include anode and cathode, and cathode consists of active material, binder, and a conductive agent. Within these cathode components, the active material is the one that is directly responsible for the specific capacity. Thus, a lot of attention has been paid to active cathode materials. As is mentioned at the beginning of this chapter, $LiNi_xCo_yMn_{1-x-y}O_2$ (NMC) materials are promising options for active cathode materials especially in the automotive industry for its high specific capacity, low cost, and low safety risk.

Instead of focusing on new ways to improve the performance of NMC materials, this research project targets on analyzing and fixing existing problems of NMC materials – degradation of electrochemical performance after contact with moisture. This is an important problem and at the same time a basic concern because it will determine how we should store the NMC materials. Even though this project is more or less focusing on a small aspect of the degradation mechanism, it will certainly help us get a more refined big picture of the issue. Through scientific experiments and reliable tests, I believe that the results of this study can offer guidance for storing NMCs and, potentially, other materials that have the correspondent properties to the degradation problem.

1.3 Overview of Thesis

This thesis has 4 chapters: Introduction, Sample Preparation, Performance Test, and Conclusion. In Chapter 2: Sample Preparation, I will discuss the detailed plan and setup of experiments for different samples, since the results of this project are heavily based on the condition and quality of samples. In addition, this chapter classifies all the samples clearly to

prevent confusions between them, considering the big number of samples. The third chapter "Performance Test" discusses the sample tests. This includes the introduction to the test technologies, the strategy of testing, the results of tests and the analysis of test results. The last chapter is Conclusion, in which I will draw conclusions based on analysis, summarize key contributions of this thesis, discuss additional applications of this work, and propose possible future directions of study.

Chapter 2: Experiments

2.1: Sample Preparation

Sample preparation is very important for this research. Experiments need to be well designed in order to get convincing results and to have fair comparisons between results. The variables in this experiment include the molar ratio of NMC materials and the severity of moisture impact. The NMC materials with different molar ratios: (1) $LiNi_{1/3}Co_{1/3}Mn_{1/3}O_2$ (NMC111), (2) $LiNi_{0.5}Co_{0.3}Mn_{0.2}O_2$ (NMC523), (3) $LiNi_{0.6}Co_{0.2}Mn_{0.2}O_2$ (NMC622), (4) $LiNi_{0.8}Co_{0.1}Mn_{0.1}O_2$ (NMC811) were bought directly from the market, so the only variable that needs to be controlled in this experiment is the severity of moisture impact. To make the difference between samples as big as possible, I decided to separate each NMC material into three groups and store them under three different conditions respectively: (i) dry glovebox (fresh), (ii) 2% moisturized chamber (moisturized), and (iii) water (washed). The total number of samples turned out to be 12. To make it clear, a table was made to classify and name all the samples as shown below:

Table 1: Sample Classification

Material	Condition	Sample Name
NMC111	Fresh	NMC111_fresh
	Moisturized	NMC111_moisturized
	Washed	NCM111_washed
NMC523	Fresh	NMC523_fresh
	Moisturized	NMC523_moisturized
	Washed	NMC523_washed
NMC622	Fresh	NMC622_fresh
	Moisturized	NMC622_moisturized
	Washed	NMC622_washed
NMC811	Fresh	NMC811_fresh
	Moisturized	NMC811_moisturized
	Washed	NMC811_washed

All the samples were prepared and tested at the same time and conditions to ensure consistency within each sample group. The target weight of each sample after preparation is 2 grams, considering the consumption of each test. The "fresh" samples were simply stored in the glovebox and the desiccator all the time to minimize its chance of contact with moisture and air.

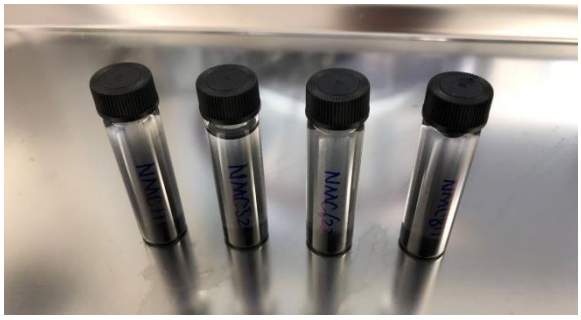

Figure 4: Samples soaked in de-ionized water

As shown in Figure 4, the "washed" samples were soaked in de-ionized water in small empty vials at room temperature for 24 hours to give the powders enough moisture impact. After 24 hours, the samples were filtered with a customized filtering system, including a funnel, a filtering flask connecting with vacuum, and a filter paper. An excessive amount of powders was

prepared for washing in case that the filter would filter out some bigger particles. The filtered powders were then dried in a furnace at 120 ℃ for another 24 hours. Lastly, the washed samples were moved to the glovebox for storage until testing.

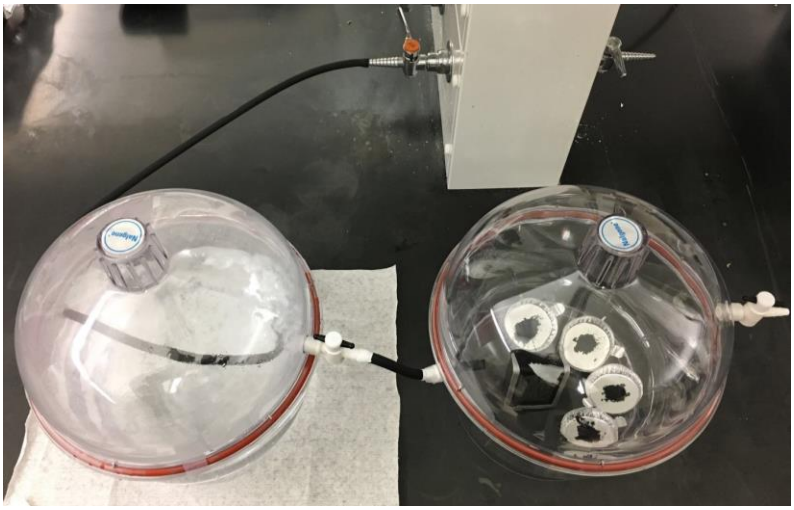

Figure 5: Experiment layout for moisturization and humidity control

The preparation of the moisturized samples took 7 days. As shown in Figure 5, a controlled moisturized condition was built with two desiccators (one half-filled with water and one containing powders), an oxygen outlet, and a Humidity Monitor. The desiccators and the oxygen outlet were linked with tubing to generate water bubbles in one of the desiccators and then transport the moisture to the other desiccator. With constant oxygen flow and room temperature, the humidity inside the desiccator should also be close to constant. Yet, we still need to monitor and record that for reference. So, a Humidity Monitor with the function of recording relative humidity and temperature was placed near the samples inside the desiccator. With a duration of 7 days, the humidity reading on the Humidity Monitor averaged about 90% RH (relative humidity). According to following equation (Lawrence, 2005),

$$T_{dp} = T - \frac{100 - RH * 100}{5}$$

where T_{dp} is dew point temperature in degree Celsius, T is room temperature in degree Celsius, and RH is relative humidity in percentage, water dew point temperature at room temperature (20 ℃) was approximated as 18 ℃. Based on the Humidity / Moisture Handbook (MAC, 1999), the corresponding percentage Moisture by Volume (% Mv) is around 2%. After moisturized in the 2% Mv condition for a week, the samples were vacuum dried in a furnace at 120 ℃ for 12 hours and stored in the glovebox for future use.

2.2: Sample Characterization

To characterize the samples, different tests were conducted, including X-ray Powder Diffraction (XRD), Fourier Transform Infrared Spectroscopy (FTIR), and electrochemical performance test from coin type battery cells. Concepts are introduced in the appendixes, and the procedures are discussed below.

The bulk structure change of the samples is a critical perspective to be investigated for our analysis. Therefore, XRD analysis was carried out on the samples using an X-ray diffractometer (Rigaku Miniflex 600) over the 2θ range of 10° - 80° with monochromatized Cu Kα radiation. Due to the relatively large number of samples and limited time, each sample was scanned for 10 minutes.

After XRD, we figured that the fast scan speed might result in an inaccurate result, so we used a technique called Rietveld refinement to manipulate the XRD data. Rietveld method refines user-selected parameters to minimize the difference between the experimental pattern and the hypothesized crystal structure model. (Ashish) The crystalline compound consists of a periodic arrangement of unit cells, which is the most basic repeat unit in the crystal, and a unit cell is defined in terms of the lattice structure and can contain single atom or atoms in a fixed arrangement. With XRD refinement, I was able to get the lattice parameters and their trends.

To find out the performance change of NMC materials after moisture impact, the electrochemical properties of the cathodes were examined by galvanostatic cycling test in LIR2032 type coin cells (half-cell). A coin cell consists of several components: base, lid, spring, spacers, anode, separator, cathode and electrolyte. The assembly is illustrated in Figure 6, where 'Lithium foil' refers to the anode, and 'Active material' refers to the cathode. The working cathodes,

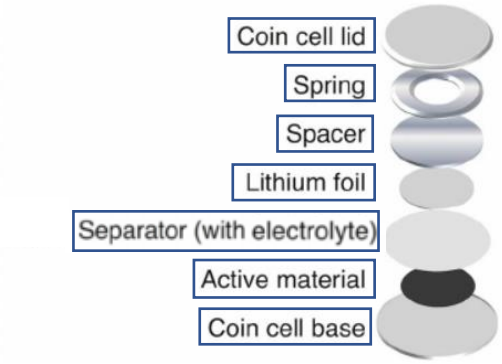

Figure 6: Coin cell assembly of the electrode half cells (Birkl, 2015)

consisting of the NMC samples: Super-P: PVdF = 85: 7.5: 7.5 in weight (with amount of NMP solvent = 2 * total mass of NMC, Super-P, and PVdF), were pasted onto Al foils as current collectors with Dr. Blade, vacuum-dried at 120 ℃ for half an hour, punched into 13.7 mm Ø round pieces, and weighed prior to use. The total amount of loaded active material for each cathode that I made ranged from 7.5 mg to 10.5 mg. In the assembly, Lithium metal was selected as the anode for half-cell, and 1.0 M $LiPF_6$ in EC/DMC = 50/50 (v/v) was used as the electrolyte.

Galvanostatic electrochemical charge and discharge tests were carried out with the Arbin Cycler in Nanotech West at room temperature. The cells were charged and discharged between 3.0 and 4.3 V by applying the current in C/10-rate for the first two cycles for preconditioning and C/3-rate for the rest. I recorded the cycling data after 9 days and got approximately 30 cycles for each coin cell. Then the cycling data was retrieved using excel and plotted with MATLAB.

After the testings about bulk structure change and performance change, we were curious about the chemical information of the samples and hoped it could give us a better view of the failure mechanism inside the material. Thus, we used a technique called Fourier-transform Infrared Spectroscopy (FTIR). The FTIR test was carried out with the Raman FTIR Microprobe from the OSU Analytical Spectroscopy Laboratory. There are a few types of sampling technique in terms of FTIR. One of them called Attenuated Total Reflection (ATR) stands out for its ease of preparation as just placing the samples on the top of a crystal.

Chapter 3: Results and Discussions

First of all, the impact of moisture contact to the particle structure and electrochemical performance was investigated. As mentioned in Chapter 2, the cell test was run under 10 and 3 C-rates for 9 days so that each cell went through about 30-35 cycles. The resultant voltage profiles are shown in Figure 7a & 7b, where I only show 8 cycles (4, 8, 12, 16, 20, 24, 28, 32) for readability.

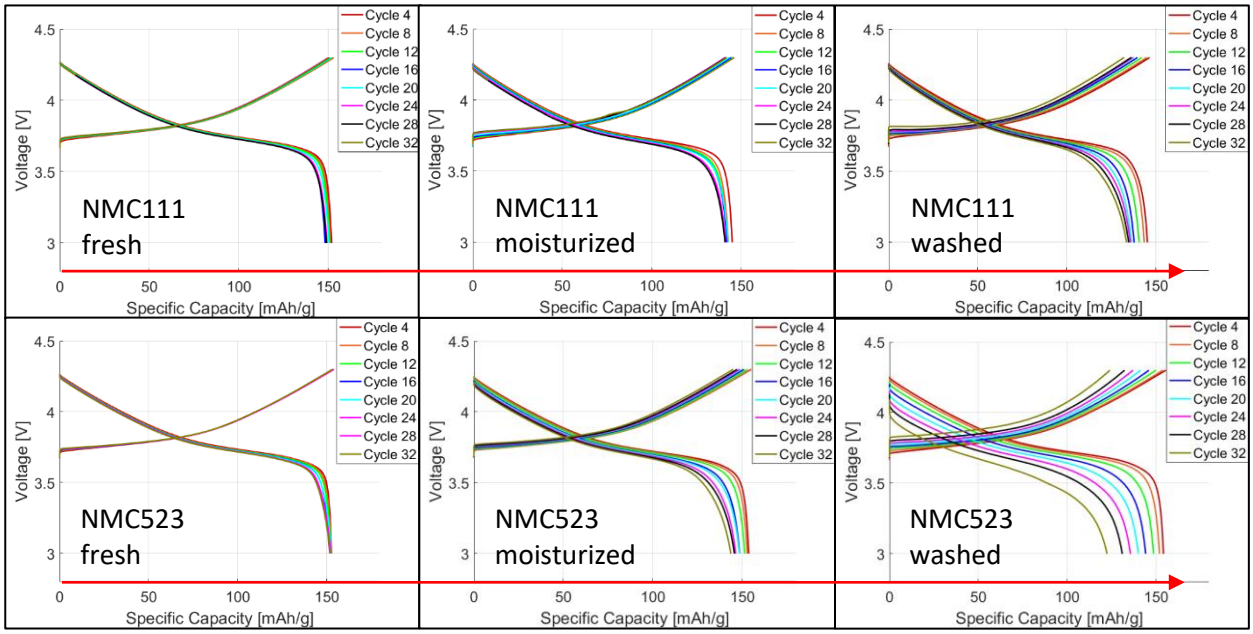

Figure 7a: Voltage profile of NMC111 and NMC523

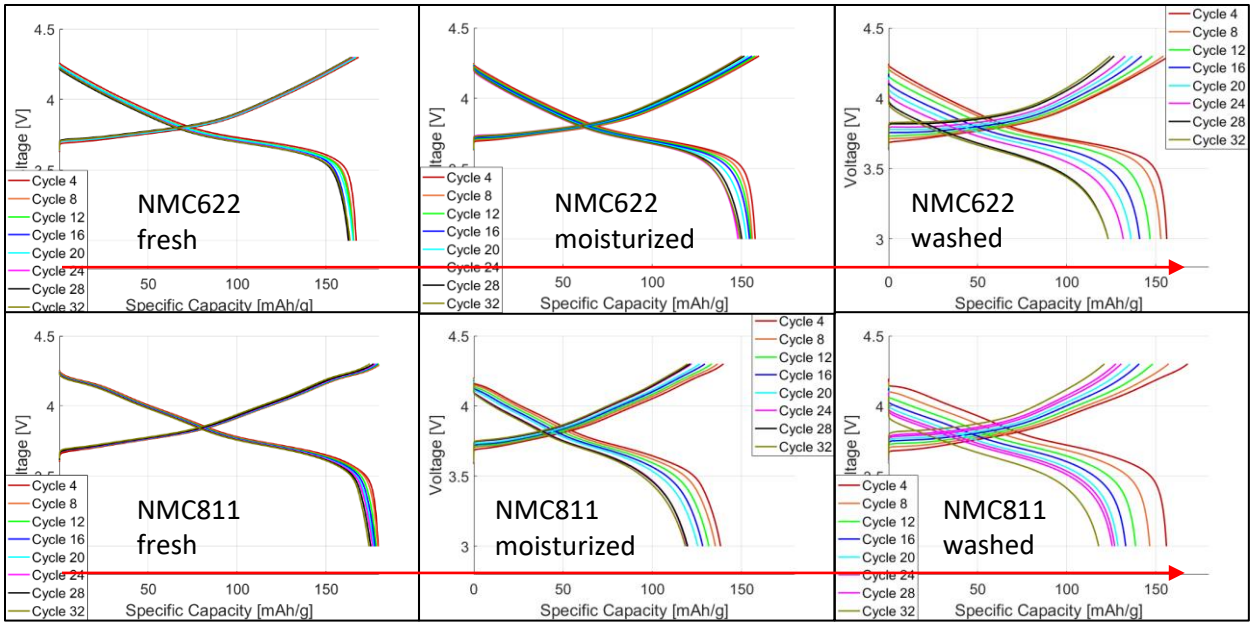

Figure 7b: Voltage profile of NMC622 and NMC811

According to these trendy plots, in terms of different conditions (follow the red arrows), the severity of capacity fading follows this trend: Washed > Moisturized > Fresh, which is illustrated by the degree of dispersion of charging and discharging lines on the plots. Take NMC811 for example, both the charging and discharging lines shift left in smaller amounts than washed NMC111 from Cycle 4 to Cycle 32, which indicates a smaller capacity fade of fresh NMC811 comparing to washed one. Also, the initial (Cycle 4) capacity follows another trend: Fresh > Washed > Moisturized. This matches with the views from literature review about the failure mechanism because the higher capacity of the washed sample may be caused by the residual

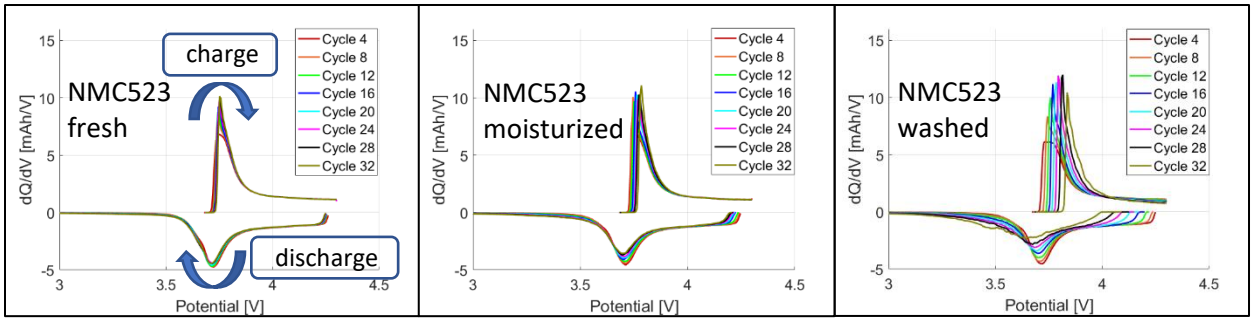

Figure 8: DQ/dV curves of NMC523

compounds being washed out. The differential capacity profile was then analyzed by plotting the dQ/dV plots.

Figure 8 above presents the dQ/dV curves of NMC523 under three conditions. Other NMCs have similar trends, so their plots are neglected here. As illustrated in the first left plot of Figure 8, the loop runs clockwise, where the top half of the curve corresponds to charging process, and the bottom curve represents discharging. The peaks in these curves indicate the potentials at which the majority of charge enters or leaves the battery. (Voltaiq, 2016) From the figure, we can find that the peaks of fresh sample hardly shifted, and the peaks of moisturized sample shift a little more compared to the fresh sample, while the peaks of washed sample shift dramatically toward higher and lower voltages. Using Ohm's Law (V = I*R), we can conclude that the internal resistance inside the cells follows this trend: Washed > Moisturized > Fresh. Also, the widening and flattening shape of the peaks of the washed sample as the number of cycles increases indicates the chemical changes to the battery materials, which is consistent with the views from the literature review and our hypothesis. Next, I compared the cycle life of the cells as shown in Figure 9 below.

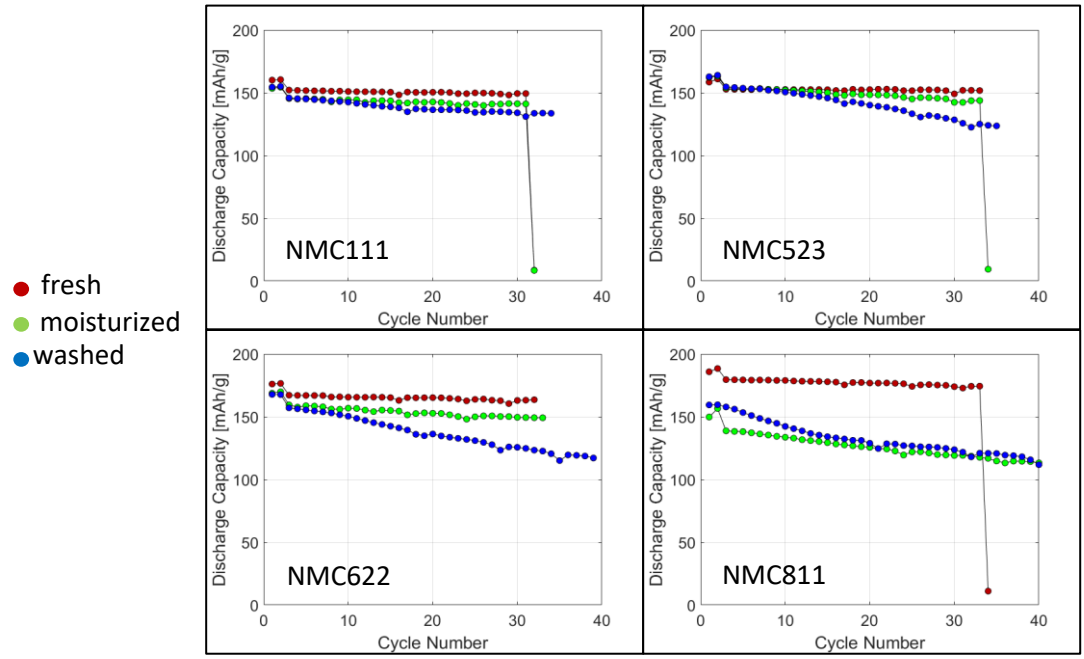

Figure 9: Cycle life of fresh, moisturized and washed samples

From the plots, it is straightforward that the moisturized sample degrades faster than the fresh sample and slower than the washed sample, which can be found by comparing the slopes of the curves. For NMC111, NMC622, and NMC811, the initial (max) discharge capacity was decreased by moisture impact. But for NMC523, the washed sample has the highest initial capacity. The possible explanation is that the fresh NMC523 sample has already been contaminated by residual compounds on the surface to some extent, and the residual compounds were washed off when soaked in water, which relives the deterioration from surface contamination. This assumption can also be used to explain why the capacity of washed NMC811 is higher than the moisturized one throughout the cycles. From the NMC811, we can also find that the washed sample did not have a rapid capacity decrease after the preconditioning cycles (first and second cycles), which means that the washed sample had a smaller impact from the construction of SEI layer. This supports our assumption because the residual compounds can thicken the SEI layer if not washed off. If this assumption is true, it can also point out that there must be some structural and chemical changes inside the particle besides the surface contamination, since the capacity fade of the washed sample is still faster even though the initial capacity is higher. The coulombic efficiency (CE) was also evaluated to check the reversibility of the cells as shown below

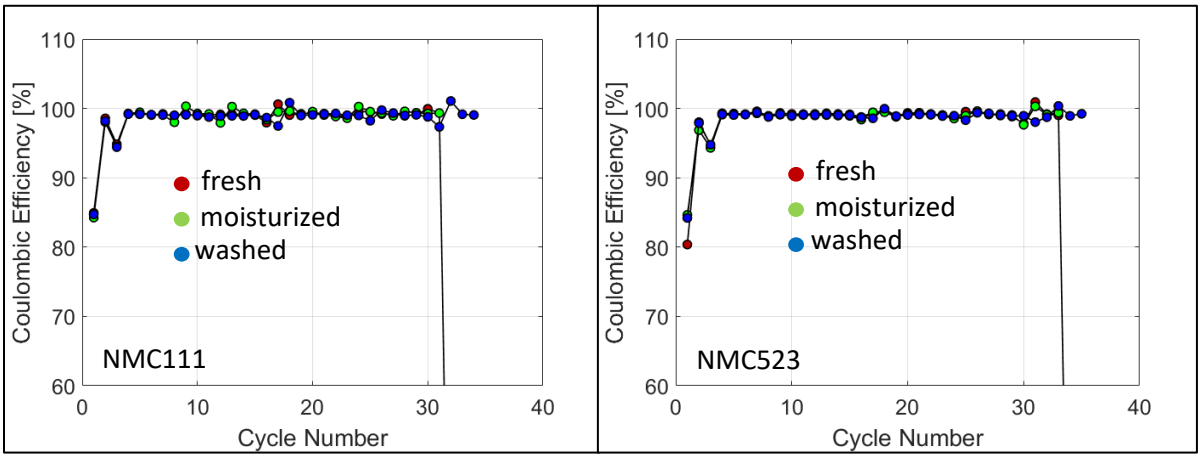

Figure 10a: Coulombic Efficiency of fresh, moisturized, and washed samples

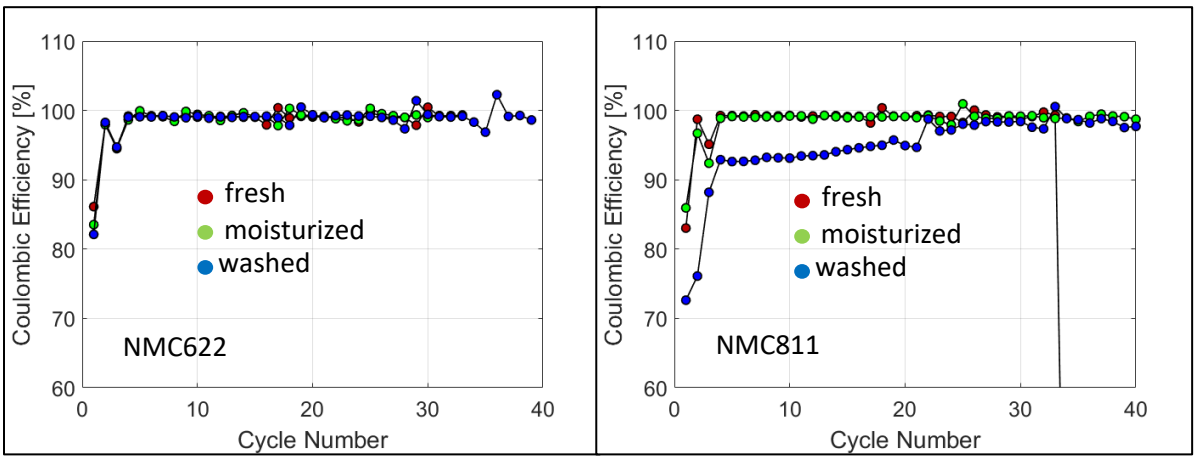

Figure 10b: Coulombic Efficiency of fresh, moisturized and washed samples

Coulombic efficiencies of fresh (red), moisturized (green) and washed (blue) samples are compared here. It is calculated as the ratio of discharged capacity to charged capacity during each cycle, and it improves with cycling in LIB. The resultant plots do not show obvious differences between curves of fresh, moisturized and washed samples. The only exception is the curve of washed NMC811, which started from a very low CE and finally got close to 100% after 25 cycles. Yang et al. discovered that the long-term CE evolution can be used to indicate the degradation rate inside a cell. A stable CE corresponds to a constant degradation rate, while a sharp decrease of the CE curve can indicate an increased degradation rate. (Yang, 2018) According to that rule, we can see that the curves of washed samples do have more sharp decreases than fresh and moisturized samples, and they do look more unstable. Thus, we can conclude from the CE data that the samples prepared in washed condition degrade more rapidly than ones prepared in other conditions.

The results from cell tests in terms of different severity of moisture impact have been covered above. As mentioned in Chapter 2, we moved forward to XRD tests to find the structural changes of the NMC samples after moisture contact. Based on literature review, there should be some changes in the crystal structure of NMC samples that are related to the degradation of

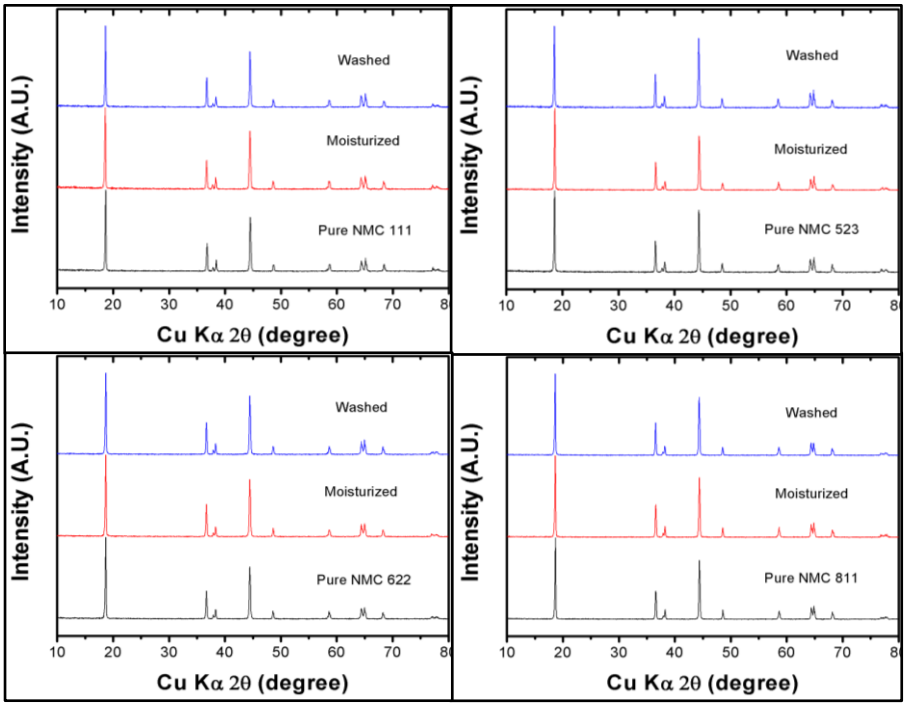

Figure 11: XRD patterns of all samples

electrochemical performance. However, the XRD patterns (Figure 11) we got was not intuitive enough to draw conclusions because the peaks hardly shift. Thus, we did the XRD refinement with Rietveld method to better interpret the XRD results. The results are shown in Table 2 below, where

Table 2: Rietveld Refinement Lattice Parameters

Sample Name	a [Å]	c [Å]	Vol [Å^3]	Rw (%)	c/a
NMC111_fresh	2.85802	14.22426	100.621	28.429	4.976963
NMC111_moisturized	2.85968	14.22948	100.775	29.158	4.975899
NCM111_washed	2.86186	14.2377	100.987	28.273	4.974981
NMC523_fresh	2.86688	14.23325	101.311	25.978	4.964718
NMC523_moisturized	2.86697	14.22841	101.282	24.888	4.962874
NMC523_washed	2.86868	14.23248	101.432	24.633	4.961334
NMC622_fresh	2.86335	14.19705	100.804	23.46	4.958196
NMC622_moisturized	2.86621	14.21036	101.1	22.656	4.957892
NMC622_washed	2.86715	14.20887	101.156	22.003	4.955747
NMC811_fresh	2.8674	14.18187	100.981	20.913	4.945899
NMC811_moisturized	2.86775	14.19184	101.077	20.484	4.948772
NMC811_washed	2.87089	14.20092	101.363	18.867	4.946522

lattice parameters *a* [Å] and *c* [Å] are the widths and heights of the unit cells respectively. It is obvious that the width and total volume of each type of NMC unit cell are increased as the severity of moisture impact increases, which means that the structural size of the NMC crystals was expanded after moisture impact.

As mentioned in the introduction, the expansion of the lattice dimensions is associated with surface migration of Li-ions from bulk from a moisture attack, which leads to the production of LiOH and Li_2CO_3 at the surfaces. To analyze the surfaces, the chemical changes of the samples were tested using FTIR with ATR sampling technique. The resultant FTIR pattern of NMC811 as a representative of various NMC materials is presented in Figure 12.

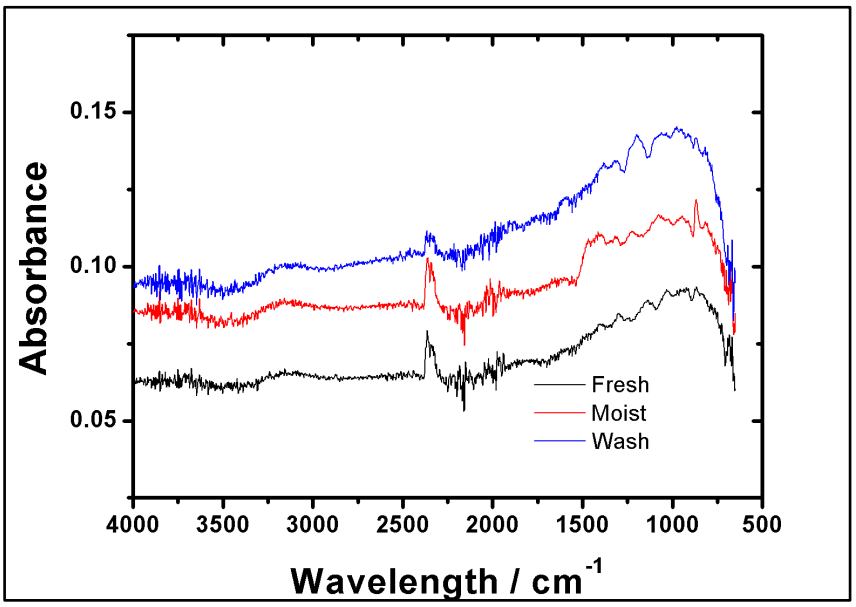

Figure 12: FTIR spectrum of NMC811

According to the library, the peaks located at 2363 and 3435 cm^{-1} are assigned to the stretching vibration of -OH and CO_2, respectively. The -OH peaks look similar between three samples, while the CO_2 peaks are quite different. This could suggest that most of the LiOH were further reacted to Li_2CO_3, so no significant peak change occurred corresponding to the vibration of -OH. We can also observe that the CO_2 peak values follow this trend: Moisturized > Fresh >

Washed. The moisturized sample has a bigger amount of CO_2 than a fresh sample, which could indicate the increased amount of Li_2CO_3 under moisturized condition. The low CO_2 the peak of the washed sample can be explained by the dissolution of LiOH in water without their conversion to Li_2CO_3. In addition, Li_2CO_3 has limited solubility in water (10 times less than that of LiOH).

With all the results above been analyzed, it is sufficient to validate that moisture impact has a noticeable effect to the NMC materials with regard to their structural, chemical, and electrochemical changes and these changes can result in significant deterioration of capacity and cycle life. Next, we will move on to the next topic: Effect of Ni content on NMC's degradation after moisture contact. The analysis is done with the same tests and results but in different aspects.

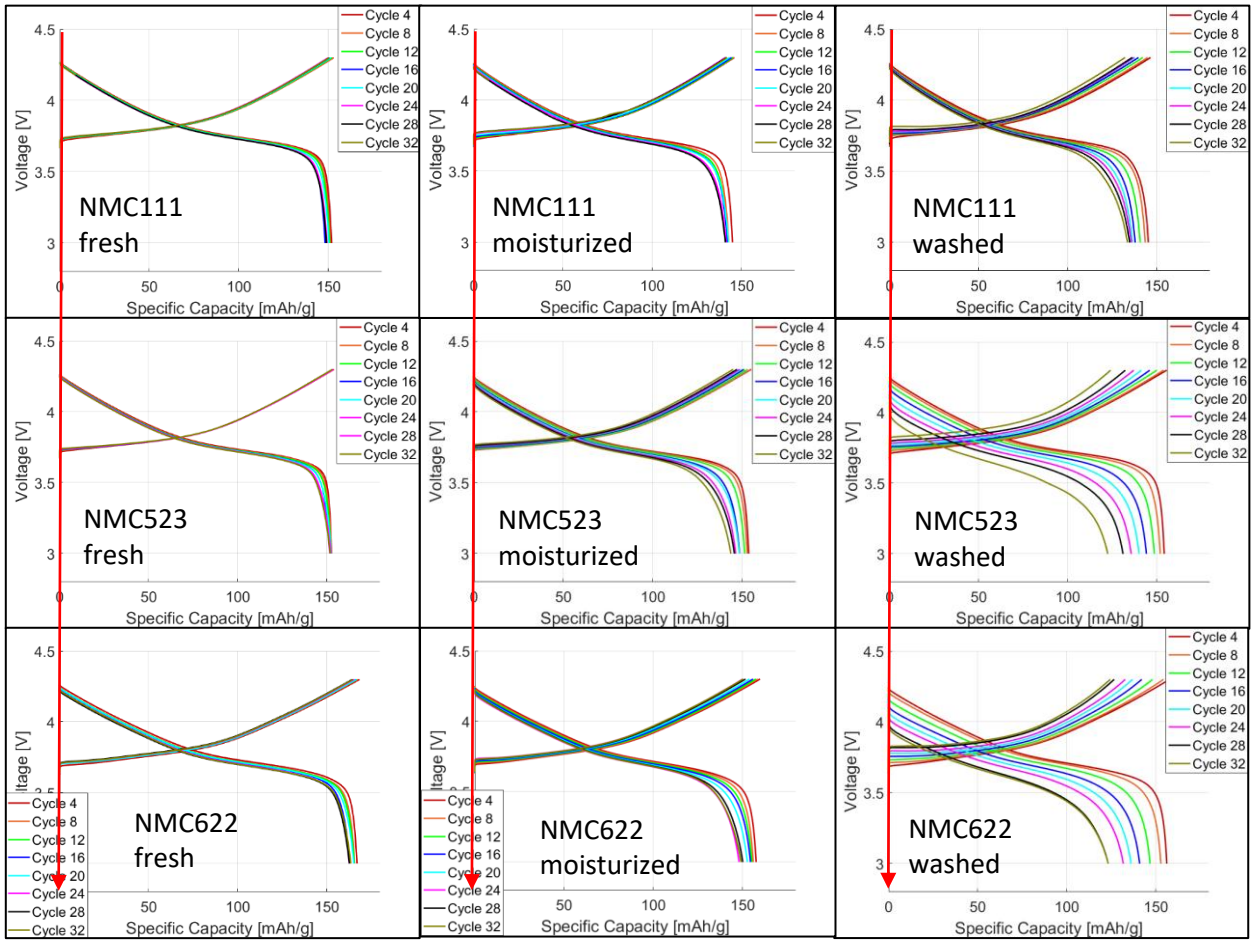

Figure 13a: Voltage profile of NMC111, NMC523 and NMC622

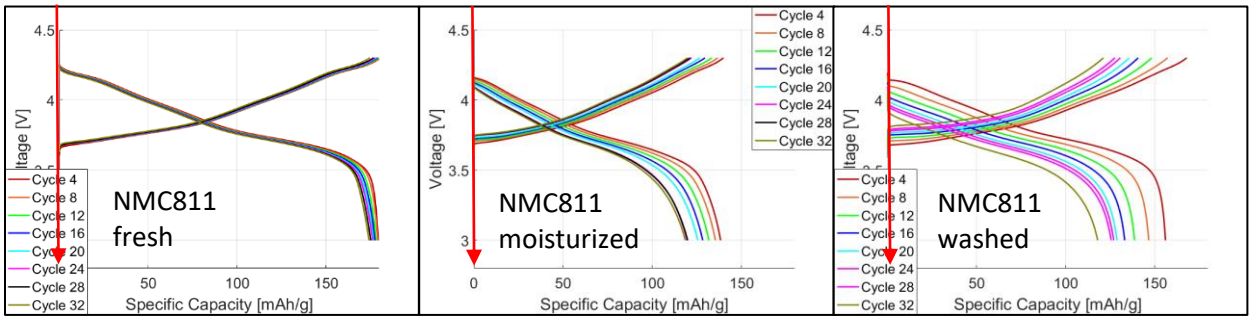

Figure 13b: Voltage profile of NMC811

Following the same sequence, the first result we are going to discuss is the voltage profile. This time, the comparisons are made between different NMCs under same conditions. Following the red lines, we can observe that the cells made from NMCs with higher Ni content have both more rapid capacity fade during cycling and a more obvious decrease of maximum capacity than those with lower Ni content. Based on this, we can easily draw the conclusion about the relationship between Ni content and capacity degradation: higher the Ni content is, the faster the capacity fades, and the more the maximum capacity decreases.

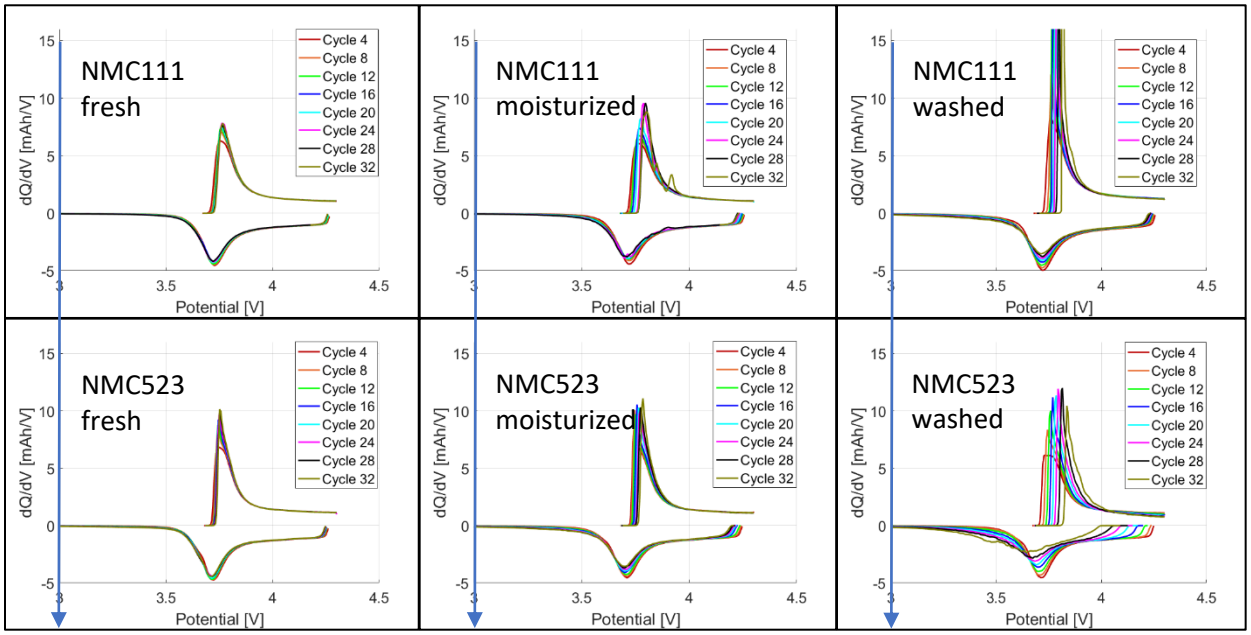

Figure 14a: DQ/dV curves of NMC111 and NMC523

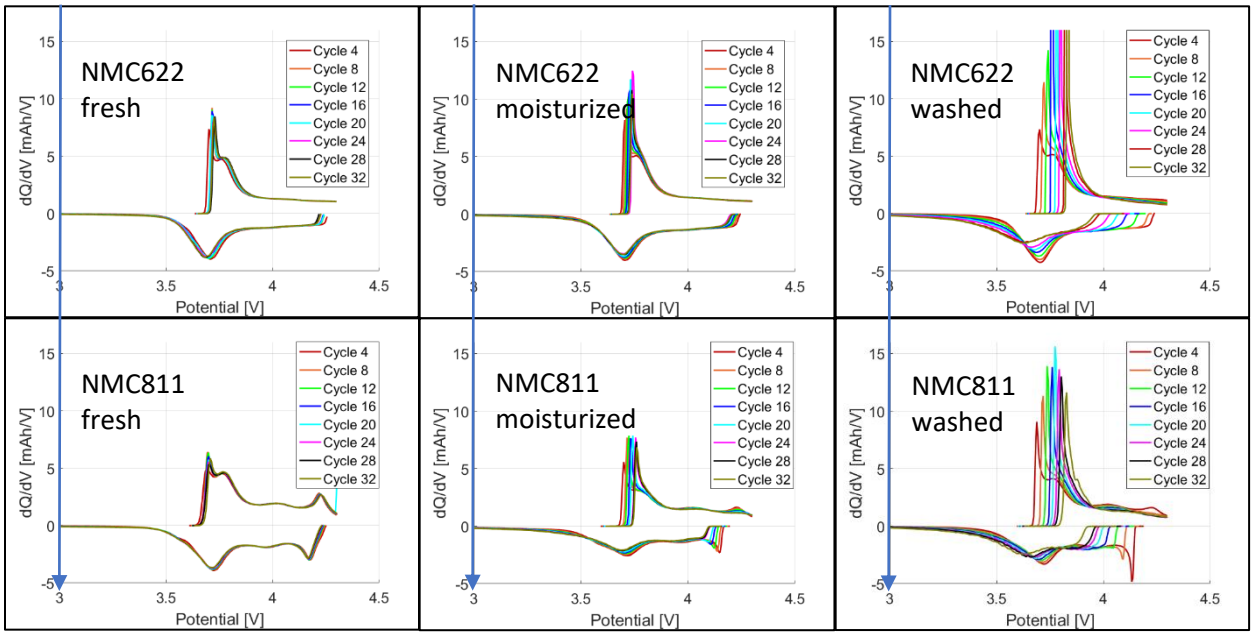

Figure 14b: DQ/dV curves of NMC622 and NMC811

Figure 14 a & b shows the complete results of dQ/dV plots. Following the blue lines, under same conditions, we can observe that the peaks of the NMC811 samples shift more dramatically to the higher and lower voltages than that of other samples. Also, the difference of peak shift distance between moisturized and washed samples suggests that the NMC811 has a more dramatic change in moisture impact. Based on these results, we can say that there must be more chemical changes in the samples with higher Ni contents.

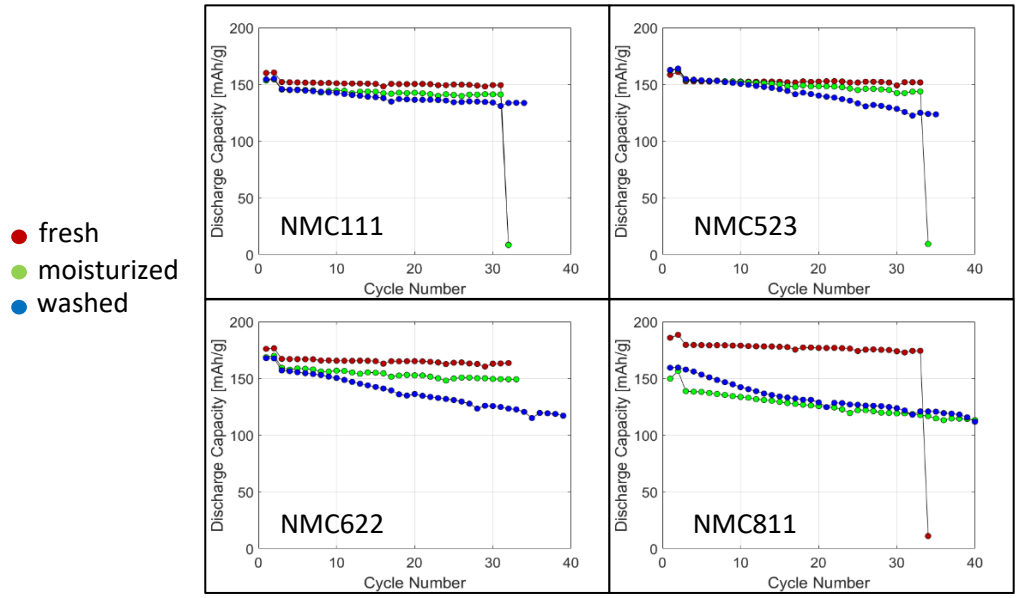

Figure 15: Cycle life of fresh, moisturized and washed samples

Using the same figure for cycle life analysis, if we compare the changes between curves within each plot, we can find that the samples with higher Ni content have bigger changes between their sub-samples. For example, curves of NMC622 are more discrete than those of NMC523. That trend suggests that samples with higher Ni content will degrade faster than ones with lower Ni content after moisture impact.

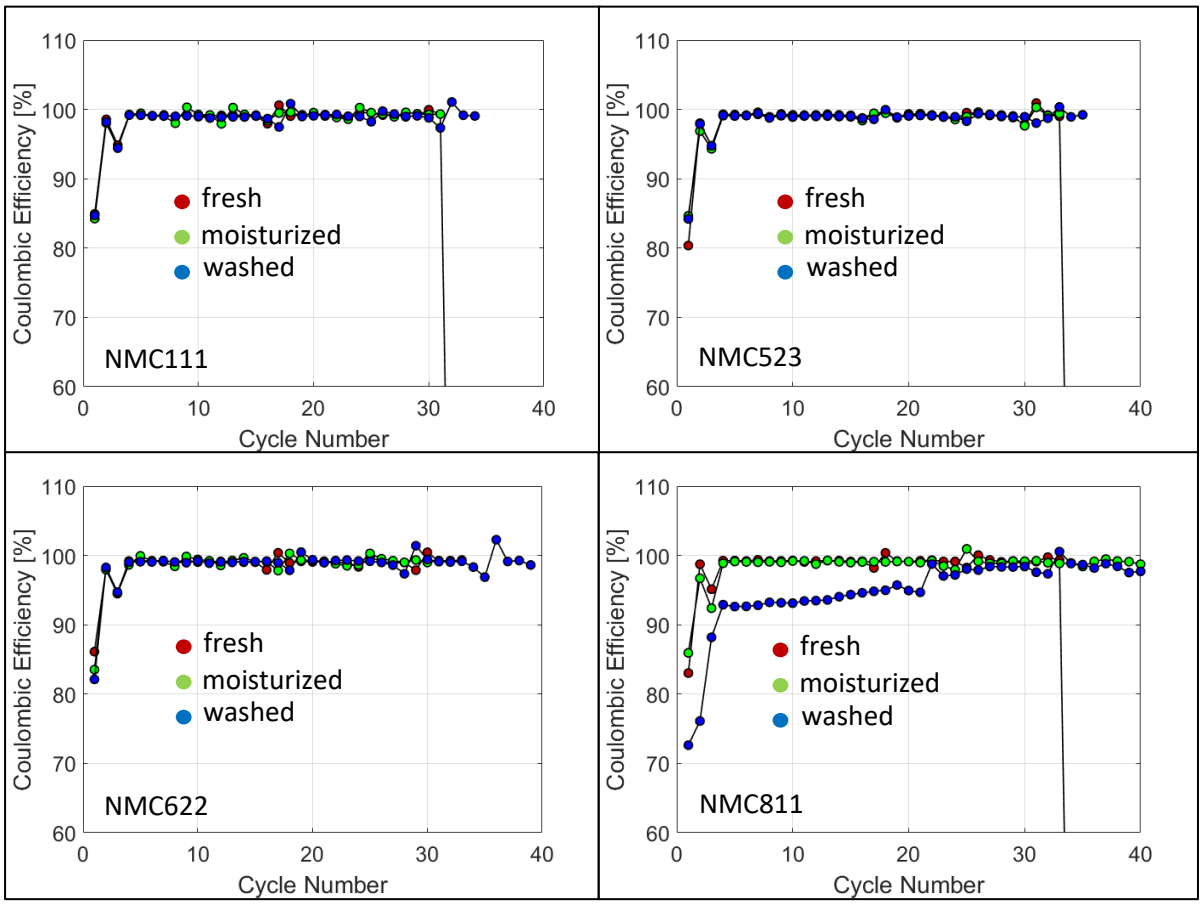

Figure 16: Coulombic Efficiency of fresh, moisturized and washed samples

Still using the same figure as the last section, the coulombic efficiency plots work better in comparing between NMCs. NMC811 is obviously more unstable and has more sharp declines of CE during cycling. If we compare between curves in each NMC, we can also see that NMC811 has greater differences between different conditions. This behavior also suggests that high Ni NMC degrades more rapidly than others.

To see the trend of dimensional changes more intuitively, I plotted the XRD refinement results as

shown in Figure 17, in which ‘non-treatment’ is equivalent to ‘fresh’.

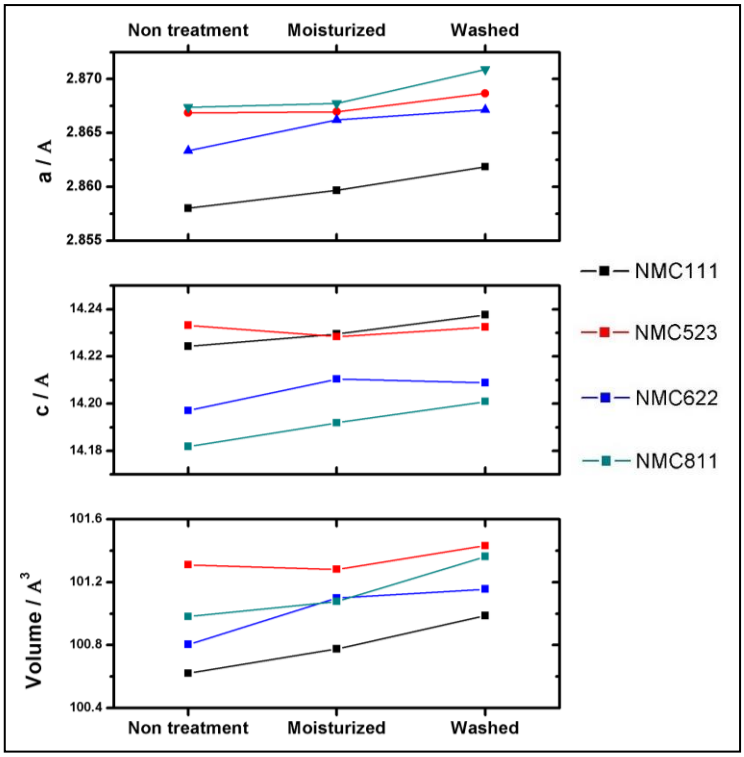

Figure 17: Rietveld refinement dimension trending curves

From the plots, we can clearly see the trend of dimensions of the crystal structure. Since the structure is in a layered shape, we are going to discuss mostly the lattice parameter *c* (parallel to height direction in the layered structure). Except for the fresh NMC523 sample, the curves of the NMCs are following this trend: NMC111 > NMC622 > NMC811. The exception of NMC523 actually matches with the assumption in the previous cycle life analysis (pg.14, line.5) that the fresh NMC523 sample may have already been contaminated by residual compounds on the surface to some extent. If that is true, the correct trend of heights is likely to be NMC111 > NMC523 > NMC622 > NMC811. This trend matches with my hypothesis. The logic is as follows: The vacant Li sites can increase the height of unit cells due to the repulsion force between O^{2-} ions blocked by Li^{+} before. The higher amount of Ni will result in more Ni^{2+} being generated and occupy the

vacant Li sites, thus blocking the repulsion between O^{2-} ions again, and shorten the height of the unit cell.

Chapter 4: Conclusion

Our results demonstrate a clear trend that electrochemical performance of NMC deteriorates with increasing severity of moisture attack (i.e., from moisture contamination in the air to immersing in water). This change in performance is accompanied by changes in chemical composition (e.g., Li-extraction to the surface) and resulting volume expansion of bulk structure. FTIR spectra confirm the presence of LiOH and Li_2CO_3 in NMC. In addition, we performed a systematic investigation on the effect of Ni contents in NMC on the electrochemical performances. With increasing Ni contents from NMC111 (0.333 stoichiometric amount of Ni) to NMC811 (0.8 stoichiometric amount of Ni), the rate of capacity fading and internal cell-impedance increase. These results suggest that NMC with high-Ni contents will require additional caution in the manufacturing process such as a strict regulation for the humidity in the air. Or, it would be necessary to tune the chemistry of the high-Ni NMC (e.g., NMC811) that can effectively resist moisture.

Chapter 5: Future Work

Although our study clearly demonstrates the effect of moisture on the performance of NMC, we still need to investigate further to find a fundamental degradation mechanism of NMC. For example, structural and surficial analysis of moisture-contaminated NMC needs to be reinforced. The quantification of surface species by using FTIR is not obvious and needs more elaboration in a future study. Also, we plan to observe the surface species by using high-resolution scanning

transmission electron microscopy (STEM) technique. Based on the results, our future interest will be directed toward tuning the chemistry of the high-Ni NMC that can effectively resist moisture by substitution or surface coating.

Appendix A: XRD

X-ray Powder Diffraction (XRD) is a non-destructive analytical technique that is primarily used for structural and phase composition studies of crystalline materials and can provide information on unit cell dimensions. X-ray diffraction is the elastic scattering of x-ray photons by atoms in a periodic crystal lattice, which is defined as the three-dimensional arrangement of particles as points in space. The diffracted x-rays that are in phase give constructive interference. This construction interference satisfies the Bragg's Law, which is used to derive lattice spacings,

$$n\lambda = 2d\sin\theta$$

where n is the order of reflection, λ is the wavelength of x-rays, d is the characteristic spacing between atomic planes of the crystalline compound, and θ is the diffraction angle. By scanning the sample through 2θ angles, all possible diffraction directions of the lattice should be obtained. Figure 18 shows the layout of X-ray diffraction, in which parameters d and θ are clearly marked.

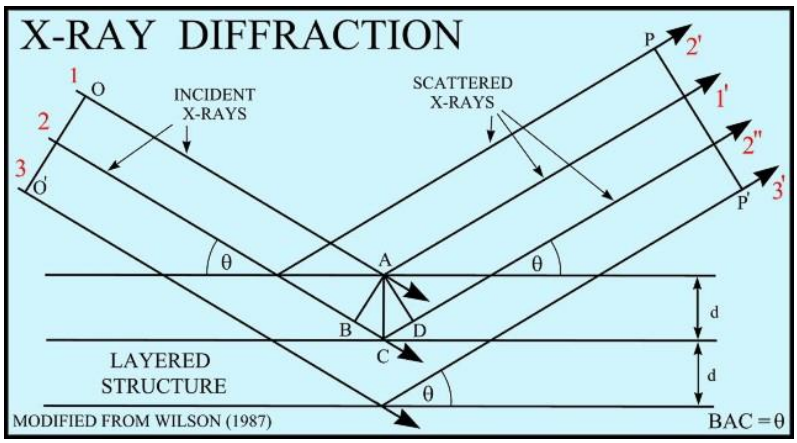

Figure 18: X-rays are diffracted by the layers of atoms (Crain, 2015)

Appendix B: FTIR and ATR

Fourier-transform Infrared Spectroscopy (FTIR) is a technique used to obtain an infrared spectrum of absorption or emission of a substance. In a regular FTIR spectrometer, an IR beam is directed onto the sample and gets partially transmitted or reflected. A detector receives a signal from the resultant radiation that comes from the IR beam. The signal is then converted to an interpretable spectrum with Fourier Transform. The patterns in such spectrums can represent the molecular 'fingerprint' of the sample; thus, samples can be quantified and identified with their chemical information because molecules exhibit specific IR fingerprints.

One of the sampling techniques of FTIR is called Attenuated Total Reflection (ATR). It is known for its ease of sample preparation. Samples are simply placed on an optically dense crystal with a higher refractive index than the sample. The IR beam is directed onto the crystal and causes

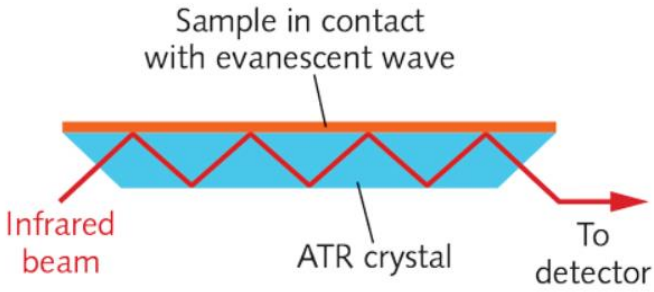

Figure 19: FTIR-ATR schematic (Dhillon, 2016)

internal reflectance. The reflectance then forms an evanescent wave which extends into the sample. The regions of the evanescent wave that penetrated the sample get attenuated because the energy is absorbed by the sample. The attenuated beam is then collected by the detector as it exits the crystal. Figure 19 above illustrates the schematic of FTIR-ATR.

Reference

[1]. Nishi, Y. The development of lithium ion secondary batteries. Chem Rec, 1, 406–413 doi: 10.1002/Tcr.1024 (2001).

[2]. Jaephil Cho et al. Nickel-rich layered lithium transition-metal oxide for high-energy lithium-ion batteries. Angew. Chem. Int. Ed. 54, 4440-4457 doi: 10.1002/anie.201409262 (2015).

[3]. H. S. Liu, Z. R. Zhang, Z. L. Gong, and Y. Yang, Origin of Deterioration for $LiNiO_2$Cathode Material during Storage in Air. *Electrochem. Solid-State Lett.*, 7, A190-A193 doi: 10.1149/1.1738471 (2004)

[4]. Xun-Li Wang et al. Visualizing the chemistry and structure dynamics in lithium-ion batteries by in-situ neutron diffraction. Scientific Reports, 2, 747 doi: 10.1038/srep00747 (2012)

[5]. J. -h Park et al. Stability of $\mathbf{LiNi_{0.6}Co_{0.2}Mn_{0.2}O_2}$ as a cathode material for Lithium-ion batteries against air and moisture. Bull. Korean Chem. Soc. 37, 344-348 doi: 10.1002/bkcs.10679 (2016)

[6]. Chaofeng Liu et al. Understanding electrochemical potentials of cathode materials in rechargeable batteries. Materials Today, 19, 2, 109-123 doi: 10.1016/j.mattod (2016)

[7]. Lawrence, M.G. The relationship between relative humidity and the dew point temperature in moist air: A simple conversion and applications. Bull. Am. Meteorol. Soc. 2005, 86, 225–233 doi: 0.1175/BAMS-86-2-225 (2005)

[8]. Machine Applications Corporation. The MAC Humidity/Moisture Handbook (1999)

[9]. Ashish Garg. A Brief Introduction to Rietveld Analysis of XRD Patterns. Retrieved from: https://www.iitk.ac.in/tkic/workshop/XRD/ppt/Prof%20Garg/AshishGarg_Rietveld.pdf

[10]. C. R. Birkl, E. McTurk, M. R. Roberts, P. G. Bruce, and D. A. Howey, “A parametric open circuit voltage model for lithium-ion batteries,” Journal of The Electrochemical Society, vol.

162, no. 12, pp. A2271–A2280. (2015)

[11]. Voltaiq. Electrochemistry Data Hidden In Your Time Series Data: dQ/dV. Retrieved from: https://www.voltaiq.com/blog/electrochemistry-data-hidden-in-your-time-series-data-dq/dv (2016)

[12]. Yang, F., Wang, D., Zhao, Y., Tsui, K-L., & Bae, S. J. (2018). A study of the relationship between coulombic efficiency and capacity degradation of commercial lithium-ion batteries. Energy, 145, 486-495. DOI: 10.1016/j.energy.2017.12.144 (2018)

[13]. Crain's Petrophysical Handbook. Retrieved from: https://www.spec2000.net/09-xrd.

[14]. Dhillon, H., De Wit, H., Dodson, J. Spectroscopy: CVD diamond attenuated-total-reflection prisms benefit FTIR spectroscopy. Laser Focus World (2016)